Design of Fuzzy and HBCC based Adaptive PI Control Strategy of an Islanded Microgrid System with Solid-Oxide Fuel Cell

S.Choudhury *‡, P.K.Rout *

* Department of EEE, Siksha 'O' Anusandhan University, Odisha,India

(subhashree3@gmail.com, pkrout_india@yahoo.com)

‡ S.Choudhury; P.K.Rout, Siksha 'O' Anusandhan University, Odisha,India, Tel: +91 8093162126,

subhashree3@gmail.com

Received: 04.08.2016 Accepted: 19.09.2016

Abstract- In Microgrid environment distributed generating (DG) systems are more vulnerable to load disturbance and fault during islanded mode of operation. So it is necessary to maintain the stability of the islanded system during the transient conditions. This work mainly focuses on the performance of the proposed approach Adaptive PI controller (APIC) applied on an islanded Microgrid system integrated with a Solid-Oxide Fuel Cell (SOFC) DG. A P-V control strategy is implemented for maintaining the stability of the system to restore the continuity, reliability and power quality under linear load, non-linear load and voltage variation. The SOFC establishes the modulation technique with a PWM method. The performance of the proposed controller is further improved by using an adaptive hysteresis band calculation (HBCC). A comparative result of proposed algorithm with Conventional PI and Fuzzy PI are demonstrated and its enhanced control performance is presented on the basis of settling time, rise time, peak overshoot, peak undershoot and damping oscillations of system parameters. A detailed mathematical model of the SOFC stack controller and other system components are presented in detail and are simulated in MATLAB/SIMULINK environment.

Keywords Distributed Generation (DG), Adaptive PI (API), Hysteresis band Current Controller (HBCC), Voltage Source Converter (VSC), Solid-Oxide Fuel Cell (SOFC), Mamdani-Fuzzy Logic Controller (M-FLC), Pulse Width modulation (PWM).

1. Introduction

Distributed Generation (DG) has given rise to a new solution in power generation to provide reliable and secure electricity supply to the consumers. The integration of small DGs enables to achieve reduction of transmission losses, improvement of power quality, better demand response and continuity of supply even after being disconnected from the main grid. However, due to the intermittent and the uncertainty caused by environmental factors, and highly non linear dynamics of DG system, it is difficult to integrate renewable energy sources in Microgrid environment. This is the reason why various operational issues related to voltage control, power control, fault integration and power loss minimization has to be solved in order to integrate DGs into the distribution network[1-2].

At present scenario SOFC is expected to show a major role for use as DG source in future Microgrid environment. At output, DC voltage is produced and the SOFCs are integrated to local loads through power conditioning units such as DC/AC inverters. On compared with other DG technologies, such as wind and photovoltaic (PV) generation, SOFC has the advantage of fast start up time, load degradation due to corrosion and can be located at any site in a Microgrid system having no geographical limitations[3]. Because of its abundance of availability, continuity of power supply, cheap maintenance and non-toxic emission, SOFC is gaining popularity in recent time. It has been observed that SOFC can provide reliable power supply under steady state condition, but it fails to do the same under electrical load transients as fast as desired by the system. This is mainly due to slow internal electro-chemical and thermodynamic

behavior of the cell. So it is necessary to investigate and analyze the transient properties of SOFC cells to enhance their performance under different operating conditions such as linear load, non-linear load and voltage variations. An attempt has been made in this work to design an appropriate controller to address the above issues.

In the recent past various controllers have been reported in the literature on SOFC and most of them are restricted to only steady state modeling and operation. These studies do not investigate the dynamic performance of the SOFC and also based on some empirical equations. Several control strategies have been proposed based on PI controller to deal with DG operation. However, the PI controllers are needed to be tuned offline with the change of operating conditions and it lacks robustness. To circumvent the above cited problem with PI controller some authors have suggested the control strategies based on fuzzy logic [4]. Even if the fuzzy logic based controllers perform better than PI controllers under uncertainty and abnormal conditions, till the performance mostly depends on the values of the fuzzy parameters. In this paper, keeping in view the advantages of both the above types of controllers, the fuzzy logic concept is used to dynamically tune the gains of the PI controller and by so the concept of constant gains are avoided.

The gains of the PI controller are dynamically tuned by FLC in the proposed adaptive fuzzy tuned PI controller. The output response in case of conventional PI controller is not accurate as it only depends on error variation. The controller based on FLC to some extent is able to give better result and robust performance compared to conventional PI controllers as it is based on both error variation and change of error. In the proposed technique the FLC is used to dynamically change the gains of the PI controller to enhance its capability to damp the system oscillations and wider the robustness to control.

The major contributions of this work are:

I. Adaptively changing the gains of the PI controller based on fuzzy logic.

II. Investigating the dynamic response of SOFC under very often occurred practical operating conditions like change of linear and non-linear load, and voltage variation.

III. A comparative result is demonstrated to justify the performance of the proposed controller compared to conventional PI and FLC

IV. The modulation technique for the SOFC is established with a simple PWM technique

V. The performance of the API controller is further enhanced by using an adaptive HBCC.

The rest part of the paper is organized as follows. Section 2 presents a detailed mathematical modeling of SOFC and other integrated system components. The description of conventional PI, Fuzzy based and proposed API based controller strategy is given in Section 3. It also describes a simple PWM technique for the SOFC whose controller action is enhanced by an adaptive HBCC. Simulation results and a comparative analysis and discussion are enumerated in Section 4. At last the conclusions from the entire study are drawn in Section 5.

2. Mathematical Design Approach of PV System

The architecture of the Microgrid system with SOFC is illustrated in Fig.1. A detail explanation on modeling of various components is as follows.

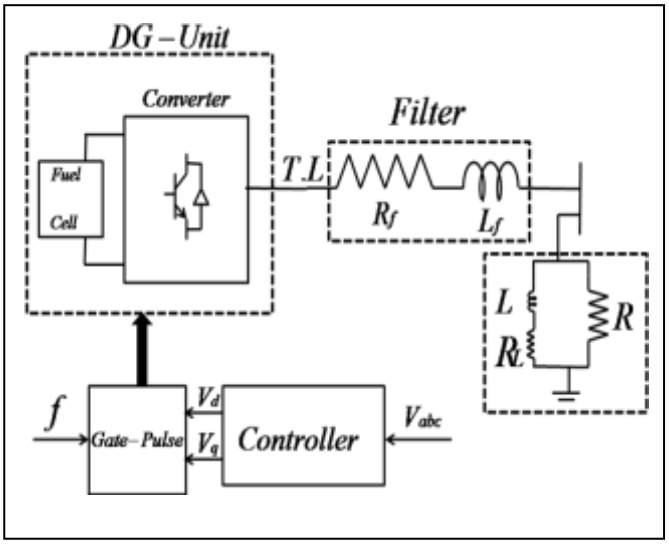

Fig.1. Architecture of Islanded Microgrid System with SOFC as source

2.1 Modelling of VSI

A VSI based 6-leged, 3-phase bridge converter is used for the control of power from source to load. The mathematical modeling of the VSI portraying its operation is presented in equation (1-6) in natural (abc) frame of reference as depicted in Fig.2. [5].

$$S_a = 2S_1 - 1 \tag{1}$$

$$S_b = 2S_3 - 1 \tag{2}$$

$$S_c = 2S_5 - 1 \tag{3}$$

$$V_{ai} = \frac{2}{3} * \frac{V_{dc}}{2} * S_a - \frac{1}{3} S_b - \frac{1}{3} S_c \tag{4}$$

$$V_{bi} = \frac{2}{3} * \frac{V_{dc}}{2} * S_b - \frac{1}{3} S_a - \frac{1}{3} S_c \tag{5}$$

$$V_{ci} = \frac{2}{3} * \frac{V_{dc}}{2} * S_c - \frac{1}{3} S_a - \frac{1}{3} S_b \tag{6}$$

Where S_1, S_3, S_5 are the switching states of the positive switches of the inverter; S_a, S_b, S_c are the three phase

switches; V_{ai}, V_{bi}, V_{ci} are the inverter output voltage and V_{dc} is the inverter DC link voltage.

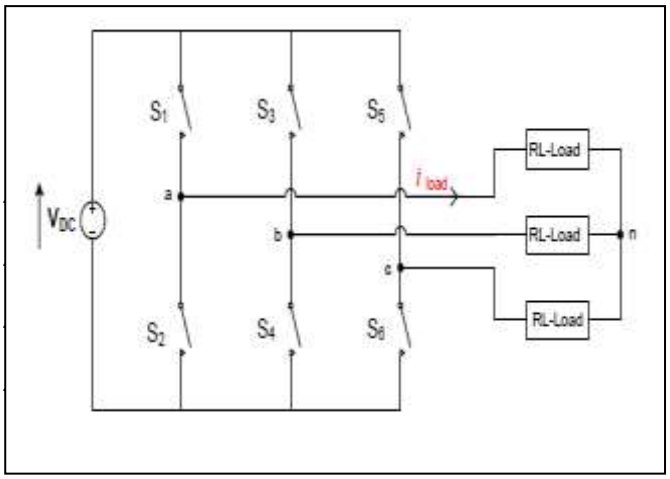

Fig.2. Structure of VSI

2.2 Modelling of Transmission Line

The 3-phase converter currents and voltages are decomposed to 2-phase (d-q synchronous rotating frame) by the '*park's transformation'* as represented in equation (7). The d-q axis line current component (i_d, i_q) can be calculated using '*park's transformation'* as follows [6].

$$\begin{bmatrix} i_a \\ i_b \\ i_c \end{bmatrix} = \sqrt{\frac{2}{3}} \begin{bmatrix} \cos(\theta) & -\sin(\theta) & \frac{\sqrt{2}}{2} \\ \cos\left(\theta - \frac{2\pi}{3}\right) & -\sin\left(\theta - \frac{2\pi}{3}\right) & \frac{\sqrt{2}}{2} \\ \cos\left(\theta + \frac{2\pi}{3}\right) & -\sin\left(\theta + \frac{2\pi}{3}\right) & \frac{\sqrt{2}}{2} \end{bmatrix} \cdot \begin{bmatrix} i_d \\ i_q \\ i_0 \end{bmatrix} \quad (7)$$

The d-axis and q-axis voltage in terms of transmission line parameter resistance R_f and line Inductance L_f at normal operating angular frequency ω_e are represented as follows:

$$V_{di} = R_f i_d + L_f \frac{di_d}{dt} - \omega_e L_f i_q \quad (8)$$

$$V_{qi} = R_f i_q + L_f \frac{di_q}{dt} + \omega_e L_f i_d \quad (9)$$

2.3 Modelling of load

The mathematical modelling of load is represented by a simple R-L circuit as shown in Fig.3. The 2-phase load current (d-q component) are converted to 3-phase equivalent by the use of '*Clark's transformation*' as described below in equation (10).

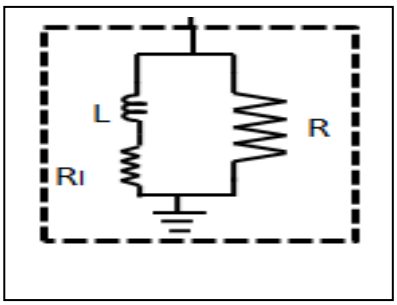

Fig.3. Circuit representation of the RL type load parallel with R load

$$\begin{bmatrix} i_d \\ i_q \\ i_0 \end{bmatrix} = \sqrt{\frac{2}{3}} \begin{bmatrix} \cos(\theta) & \cos\left(\theta - \frac{2\pi}{3}\right) & \cos\left(\theta + \frac{2\pi}{3}\right) \\ -\sin(\theta) & -\sin\left(\theta - \frac{2\pi}{3}\right) & -\sin\left(\theta + \frac{2\pi}{3}\right) \\ \frac{\sqrt{2}}{2} & \frac{\sqrt{2}}{2} & \frac{\sqrt{2}}{2} \end{bmatrix} \cdot \begin{bmatrix} i_a \\ i_b \\ i_c \end{bmatrix} \quad (10)$$

The 3-phase component of load current (i_{la}, i_{lb}, i_{lc}) can be expressed in terms of voltage components at PCC ($V_{pcca}, V_{pccb}, V_{pccc}$), load resistance R_l and load inductance L_l as follows.

$$\frac{di_{la}}{dt} = \frac{V_{pcca}}{L_l} - \frac{R_l}{L_l} i_{la} \quad (11)$$

$$\frac{di_{lb}}{dt} = \frac{V_{pccb}}{L_l} - \frac{R_l}{L_l} i_{lb} \quad (12)$$

$$\frac{di_{lc}}{dt} = \frac{V_{pccc}}{L_l} - \frac{R_l}{L_l} i_{lc} \quad (13)$$

2.4 Modeling of PLL

The 3ϕ phase locked loop (PLL) is a device which detects the phase angle θ and ω from the three phase quantity. The three phase voltage or current are the input to the PLL circuit

and the phase angle θ and system angular frequency ω of the respective voltage and current are the output. The output of the PLL is used in different controllers for conversion from three phase to two phase and two phase to three phase by using *Park's and Clark's transformation* respectively for the local measurements according to the need[7].

The control diagram of PLL indicating its functionality is represented in Fig.4. For the calculation of the output θ, two major conversions first from 3ϕ abc to α - β and then α - β to $d-q$ quantity are calculated as in equation (14-15).

$$\begin{bmatrix} V_\alpha \\ V_\beta \end{bmatrix} = \frac{2}{3}\begin{bmatrix} 1 & -\frac{1}{2} & -\frac{1}{2} \\ 0 & -\frac{\sqrt{3}}{2} & -\frac{\sqrt{3}}{2} \end{bmatrix} \cdot \begin{bmatrix} V_a \\ V_b \\ V_c \end{bmatrix} \tag{14}$$

$$\begin{bmatrix} V_d \\ V_q \end{bmatrix} = \begin{bmatrix} \cos\delta_p & -\sin\delta_p \\ \sin\delta_p & \cos\delta_p \end{bmatrix} \cdot \begin{bmatrix} V_\alpha \\ V_\beta \end{bmatrix} \tag{15}$$

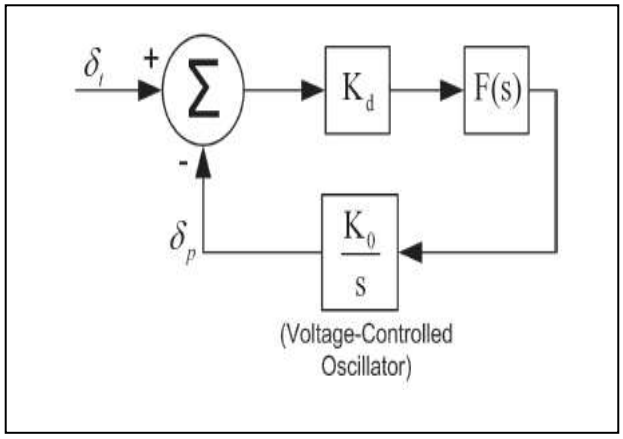

Fig.4. Control diagram of PLL

The error ($\Delta\delta = \delta_t - \delta_p$) is estimated and angle θ is calculated by making error value zero by the PI controller present inside PLL. The AC terminal voltage V_t along d-axis reference can be represented as

$$V_d = -V_t \sin(\delta_t - \delta_p) \tag{16}$$

By tuning the gain parameter of the PI controller the error can be reduced to zero. Under this condition the value of θ is calculated by integrating $\frac{d\delta_p}{dt} = \omega_p$

2.5 Modelling of BOOST Converter

The power produced by the DG unit are not enough to supply the VSI DC voltage and so this output power of the micro sources are needed to be boosted up to the required level. Generally the distributed resources are located nearer to the load centre so that the voltage level of the DG unit is within the distribution voltage range.

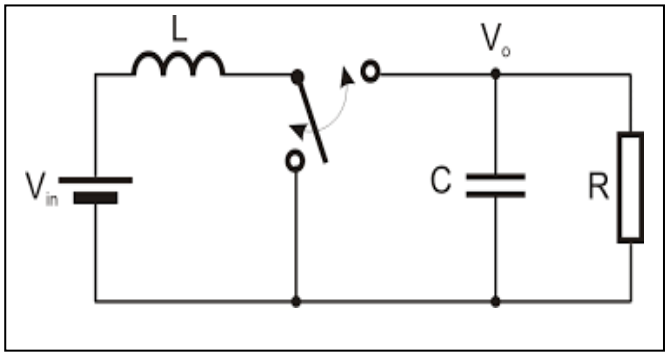

Fig.5. DC-DC boost converter

Here DC-DC boost converter is considered for the above purpose and its structure is shown in Fig.5. The mathematical modeling of boost converter is as follows[8] :

$$\begin{bmatrix} V_m \\ i_{dc} \end{bmatrix} = m\begin{bmatrix} V_{dc} \\ i_L \end{bmatrix} \tag{17}$$

Where, $m = 1 - D, D =$ duty cycle; i_L and i_{dc} are the instantaneous values. V_m is the voltage across the SOFC and V_{dc} is the capacitor voltage of DC-DC boost converter. D can be calculated as:

$$D = \frac{t_{on}}{T} = t_{on} * f_s \tag{18}$$

Where, f_s is the switching frequency of the converter; T is the time for one complete cycle; t_{on} is the TURN-ON time for one complete cycle. In case of SOFC based fuel cell the output voltage is dependent on the hydrogen and oxygen supply. As it is required a constant DC voltage for the input of the VSI, a control mechanism is needed to maintain the DG voltage level constant. A closed loop control strategy is used in the boost converter to maintain the output voltage level constant as shown in Fig.5. A PI controller is used to reduce error and to maintain the DC output voltage level constant as shown in Fig.6.

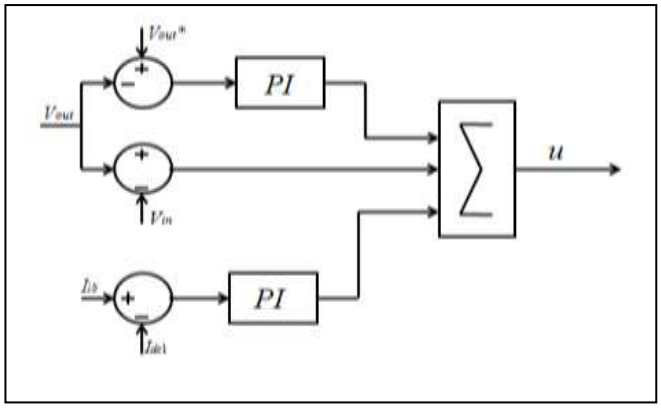

Fig.6. Control Structure of Boost Converter

3. Fuel Energy Source

Fuel cells are the electrochemical device which converts chemical energy (Hydrogen) into electrical energy by using some fuels as the raw material. A membrane electrolyte layer with porous anode and cathode on either side are the basic building blocks of the fuel cell. Fuel cells are classified on the basis of electrolyte used in the fuel cell and these includes (1) Proton Exchange Membrane(polymer)electrolyte Fuel cell(PEMFC), (2) Alkaline Fuel cell(AFC), (3) Phosphoric Acid Fuel Cell(PAFC), (4) Molten Carbonate Fuel Cell(MCFC), (5) Solid Oxide Fuel Cell(SOFC). In this paper solid oxide based FC is taken into consideration due to its highly efficient energy conversion capability and can be operated on a wide range of fuels.

3.1 Modeling of Solid Oxide Fuel Cell (SOFC)

The SOFC based fuel cell model is described in this paper having three main parts such as fuel processor, power section and power conditioner [9]. The fuel processor converts the natural gases to Hydrogen and it's by products. In power section by electrochemical reaction electrical energy is produced. Numerous Fuel cells are connected either in series or in parallel according to the output rating of the FC in power section. The power conditioner section converts the output DC power of the power section to AC form and also controls the current, voltage and frequency of the FC. The block diagram structure of the SOFC modeling is shown in Fig.7.

The detailed working process of power conditioner unit is as follows:

(a) CO is used as the Fuel gas for the SOFC by the CO-shift reaction and the by-products are fed as the input to the Fuel Cell. The CO-shift reaction is represented as follows:

$$CO + H_2O = CO_2 + H_2 \tag{19}$$

Only H_2 and O_2 enter into the fuel cell as the input.

(b) The output current of the fuel cell depends on the number of free electrons produced from the anode and cathode during the chemical reaction between the hydrogen and oxygen in the presence of ceramic electrode. The power output of the FC is limited due to the limit of current based on the availability of hydrogen. From the basic electro-chemical relationships, the molar flow of hydrogen that is involved in the reaction represents the amount of hydrogen necessary for energy conversion. This process can be mathematically expressed as follows:

$$q_{H_2}{}^r = \frac{N_0 I_{fc}}{2F} = 2K_r I \tag{20}$$

Where $q_{H_2}{}^r$, F, K_r, I_{fc} and N_0 is the molar flow rate, the Faraday's constant, the modeling constant, number of cells in series, the stack current and the number of stack of fuel cell respectively.

The Fuel utilization factor is the ratio between the fuel flow that reacts with the input fuel that enters.

$$U_f = \frac{q^r H_2}{q^{in} H_2} \tag{21}$$

Where, U_f, $q^r H_2$ and $q^{in} H_2$ are the Fuel utilization Factor, the Fuel flow and the input Fuel respectively. The amount of hydrogen fed to the FC should be utilized optimally for better overall efficiency. This process is complex because over utilization of hydrogen will cause starvation which leads to reduction of fuel cell's life and under utilization leads to reduced power efficiency. Generally, SOFC units operate within a defined limit of 80 to 90 %. This can be mathematically represented as follows:

$$I_{fcMIN} = \frac{0 \cdot 8 q_{H_2}{}^{in}}{2K_r} \le I_{fc} \le \frac{0 \cdot 9 q^{in}{}_{H_2}}{2K_r} = I_{fcMAX} \tag{22}$$

(c) From equation (22), the $q^{in} H_2$ amount can be regulated at 85% of U_f value as follows.

$$q^{in} H_2 = \frac{2K_r I^r fc}{0.85} \tag{23}$$

(d) In the SOFC the reaction takes place with the emission of H_2 at the anode O_2 and at the cathode as follows:

$$\frac{1}{2} O_2 + H_2 = H_2O \tag{24}$$

Here the ratio between the Hydrogen and Oxygen is taken as 2:1. Under normal condition the rate of water flow rH_2O value is taken as 1.145 to maintain the fuel cell pressure below 4 Kilo-Pascal (kpa). The speed of air compressor $q^{in} O_2$ should be regulated to maintain the

rH_2O value as mentioned above. The $q^{in}O_2$ can be expressed mathematically in terms of the input of hydrogen $q^{in}H_2$ as follows:

$$q^{in}O_2 = rH_2O \cdot q^{in}H_2 \tag{25}$$

(e) According to the Nernst equation the output stack voltage of the Fuel cell (V) can be expressed in terms of other system parameters including activation voltage loss and ohmic losses as mentioned in equation (26).

$$V_{fc}{}^{r} = N_0 \cdot \left[E_0 + \frac{RT}{2F} \times \ln \frac{P_{H_2} P^{\frac{1}{2}}{}_{O_2}}{P_{H_2O}} \right] - rI_{fc}{}^{r} \tag{26}$$

Where, $V_{fc}{}^{r}$ denotes Output Voltage of the Fuel cell (Volt), r denotes the electrical resistance of Fuel or ohmic loss (Ω), N_0 denotes the number of cells, E_0 denotes the voltage associated with the reaction free energy (V). Here R is the universal gas constant $\left(J/molK\right)$, T is the absolute Temperature(K), F is the Faraday constant ($Coulombs/mol$). The P_{H_2}, $P^{\frac{1}{2}}{}_{O_2}$ and P_{H_2O} represents the partial pressure of the Hydrogen, Oxygen and Water respectively $\left(N/m^2\right)$. The $I_{fc}{}^{r}$ is the output current of the Fuel Cell (A).

The total power generated (p_{fc}) by the SOFC is represented in terms of voltage (V), current (I) and number of cells N_0 as:

$p_{fc} = N_0 VI$.

The dynamic behavior of the chemical reaction can be described in terms of two time domain differential equations of two parameters partial pressure of ith species p_i (in pascals) and moles of ith species n_i(in mol) as follows:

$$\frac{dp_i}{dt} = \frac{RT}{V_{ch}} \frac{dn_i}{dt} \tag{27}$$

$$\frac{dn_i}{dt} = q_i{}^{ch} = \left(q_i{}^{in} - q_i{}^{r} \right) \tag{28}$$

Where, $q_i{}^{in}$ represents the flow of i^{th} element of the input and $q_i{}^{r}$ represents the flow of i^{th} element that reacts.

The chemical response of the SOFC is generally slow and it mostly depends upon the reaction parameter variation after a change in the flow of reactant. The time delay parameter (T_f) of the dynamic response function is taken as 5s and it is modeled as a first order transfer function as shown in Fig.7. Similarly the first order model is taken for all the dynamic response function (F_1,F_2,F_3) and time delay for different elements of F_1(for Hydrogen), F_2 (for Oxygen) and F_3(for Water) are defined as τ_{H_2}, τ_{O_2} and τ_{H_2O} respectively. The output voltage (V_{fc}) and current (I_{fc}) of the SOFC are taken as the potential difference between the anode and cathode and $I_{fc}{}^{r}$ current flow between these electrodes respectively [10-11].

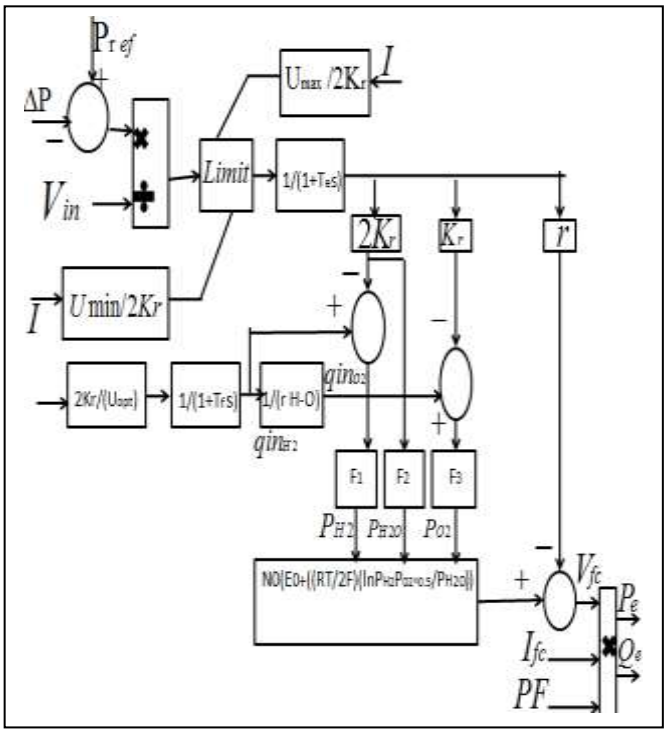

Fig.7. Working principle of SOFC fuel cell.

The rated DC output voltage of a single SOFC fuel cell is only 807.8(V). A DC-DC boost converter is used to boost up the fuel cell output voltage to acquire the desired voltage of 1500(V). The voltage, current and power at the output terminals of the boost converter are shown in Fig. (8-10).

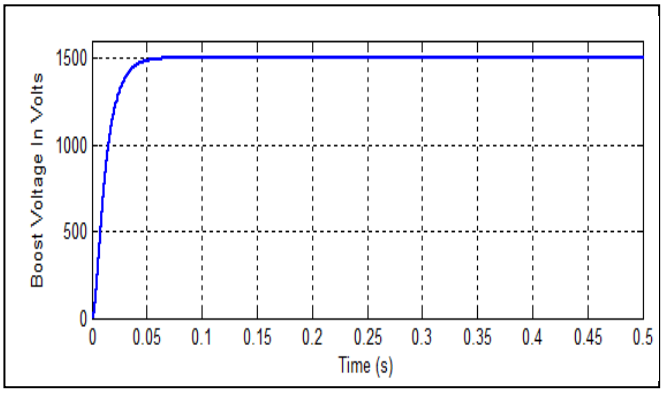

Fig.8. SOFC output voltage after Boost Converter

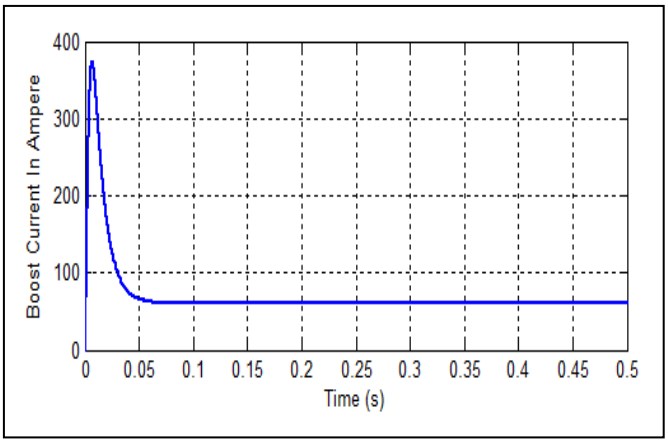

Fig.9. SOFC output Current after Boost Converter

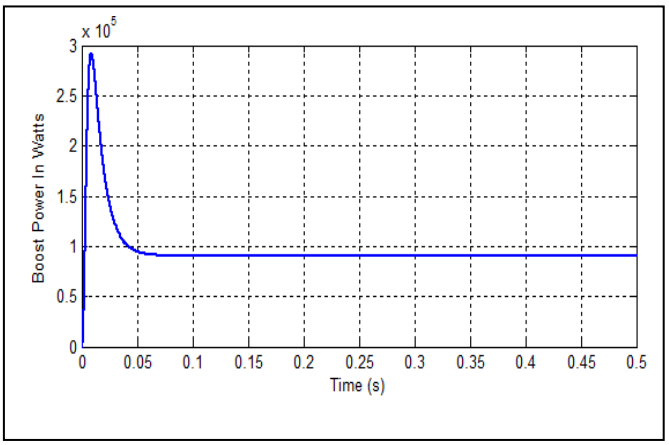

Fig.10. SOFC output power after Boost Converter

4. Control strategy of the Iislanded Microgrid System

In this study Microgrid control operating in islanding mode based on Power-Voltage $(P-V)$control strategy is designed [12]. The balance between supply and demand, maintenance of constant frequency and rated voltage, and securing the power quality are the major issues related to stability in an autonomous mode of operation [13]. Generally, in a Microgrid under regulated power supply system frequency is constant, but the operating voltage varies due to variations in load and supply. Subsequently variation of voltage leads to cumulative instability in active and reactive power transmission. The control strategy is designed for an optimal solution to Microgrid operation in view to the above problem.

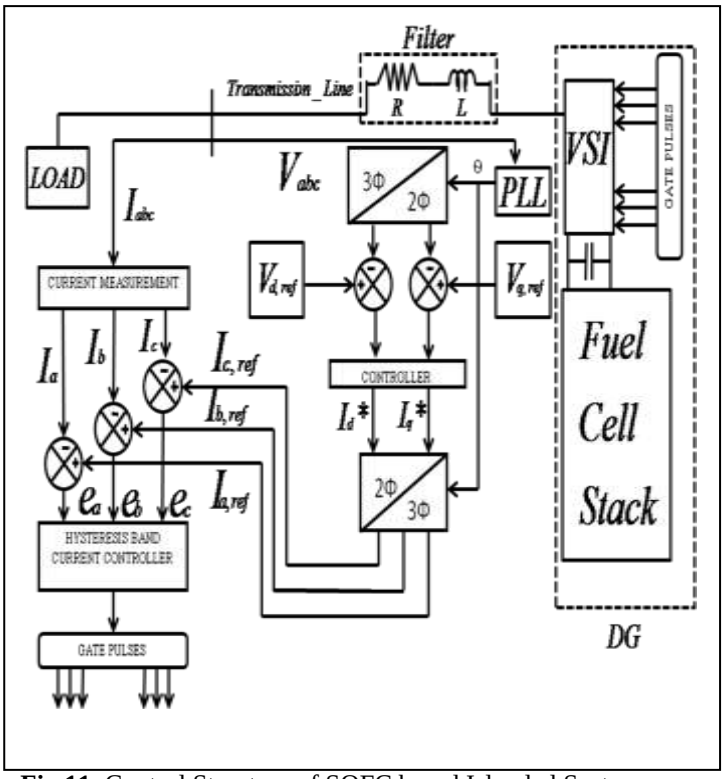

Fig.11. Control Structure of SOFC based Islanded System

The actual three phase VSI output voltage is sensed and converted to two phase d-q reference frame by '*Park's Transformation*' as mentioned earlier in equation(7). The required phase angle (θ) is sensed by the three phase PLL as explained in section 2.4 .The voltage error signals (Δevd and Δevq) of actual voltage (V_d and V_q) with respect to the reference voltage (V_d* and V_q*) are calculated as mentioned in equation(30-31).

$$\Delta evd = V_d^* - V_d \quad (30)$$

$$\Delta evq = V_q^* - V_q \quad (31)$$

These voltage error signals are then fed to the controller to generate reference currents in accordance to change in system condition [14-16]. These reference currents are further used to generate current signal error as input to HBCC for a zero error value. The control action at the output of the controller are the two phase currents I_d and I_q, and are converted to the corresponding three phase currents by using the '*Clark's transformation'* as described in section 2.3 by using the phase angle θ received from the PLL. Similarly, the corresponding errors ($\Delta e_{Ia}, \Delta e_{Ib}, \Delta e_{Ic}$) of actual currents ($I_a^*, I_b^*, I_c^*$) with respect to reference currents (I_a, I_b, I_c) are calculated.

$$\Delta e_{Ia} = I_a^* - I_a \,, \quad \Delta e_{Ib} = I_b^* - I_b \,, \quad \Delta e_{Ic} = I_c^* - I_c \tag{32}$$

These current error signals are fed to the HBCC to generate the suitable gate pulses for the PWM[17].

4.1 Modelling of PI controller

The conventional PI controller is a linear feedback control system and its control action can be expressed in terms of the system error as mentioned in the equation [18].

$$u(t) = K_p \cdot e(t) + K_i \int e(t)dt \tag{33}$$

Where K_p and K_i are the proportional and integral gains responsible for reduced steady state error, faster response and quick system oscillation damping.

4.2 Modelling of Fuzzy controller

The conventional FLC based controller is a non-linear and comparatively more robust controller w.r.t the conventional PI controller [19]. Here a mamdani type FLC is implemented for comparison. The various steps of FLC like fuzzification, fuzzy rule base, fuzzy inference and de-fuzzification are briefly discussed below [20].

4.2.1 Fuzzification

Error (e(n)) and rate of change of error (r(n)) are the two input variables of FLC which is mathematically calculated below in equation(37-38).

$$e(t) = s(t)-y(t) \tag{34}$$

$$r(t) = e(t)-e(t-1)=y(t-1)-y(t) \tag{35}$$

Where, s(t) and y(t) are the system desired value and the output of the controller in terms of time respectively.For fuzzification of e(t) and r(t) two fuzzy sets are defined. The fuzzy sets are the membership functions which are mainly of 3 types triangular, trapezoidal and bell shaped[21]. As the error can be positive and negative so the membership values are also in positive and negative range. The linguistic variables assigned to the mamdani based FLC(M-FLC) are Negative High (nh), Negative Medium (nm), Negative Low (nl), Zero (z), Positive Low (pl), Positive Medium (pm), Positive High(ph). The membership function of error and

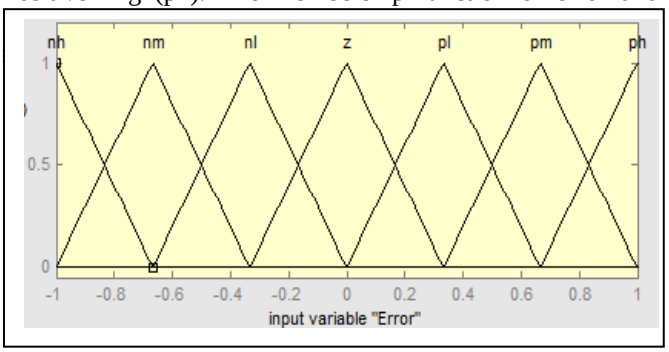

Fig.12. Membership Function of Error

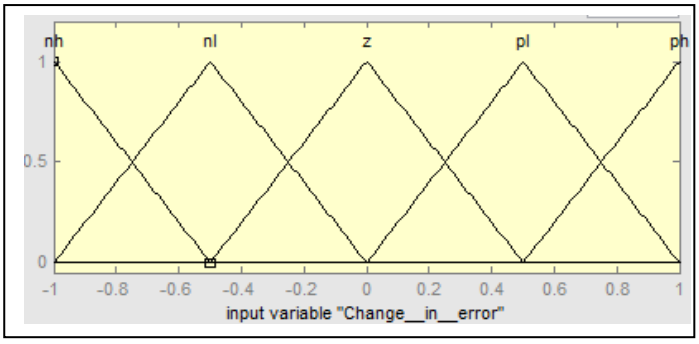

Fig.13. Membership Function of Change in Error

4.2.2 Rule Base Formulation

After the fuzzification process these results are used in the formation of rule base. The fuzzy rules are the IF and THEN statements combined by the AND operator.

Table-1. Rule Base used for the M-FLC

e / ce	nh	nm	nl	z	pl	pm	ph
nh	nh	nh	nl	nl	nl	pl	ph
nl	nh	nh	nl	nl	pl	pl	ph
z	nh	nh	nl	z	pl	ph	ph
pl	nh	nl	nl	pl	pl	ph	ph
ph	nh	nl	pl	pl	pl	ph	ph

In this study a 5×7 rule base for the M-FLC is taken into consideration. Table-I consists of Fuzzy Rule Base(FRB) which consists of 35 control rules. Fig.14 and Fig.15. shows the 3D-surface view of the control rules and the M-FLC's rule viewer respectively.

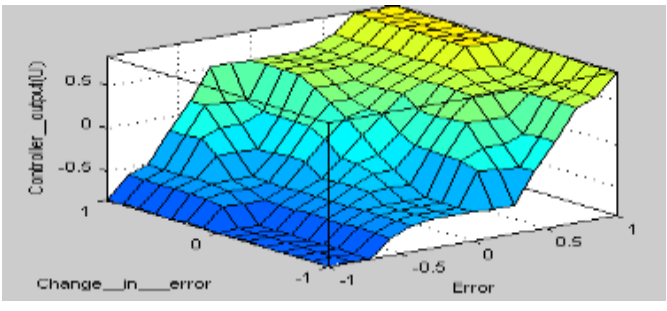

Fig.14. 3-D Surface View Of 35 Control Rules of M-FLC

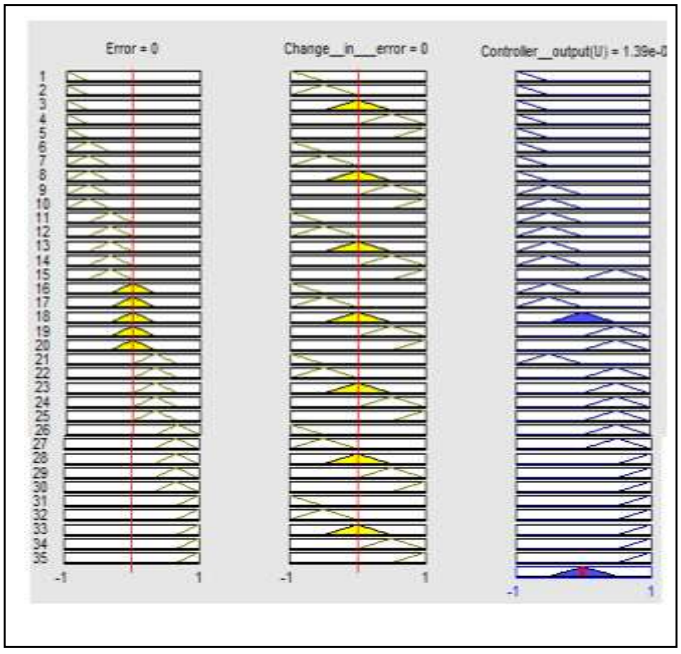

Fig.15. Rule Viewer of M-FLC Technique

4.2.3 Fuzzy Inference

The membership functions produced after fuzzification process are combined by the AND operator of the fuzzy rules and then the output membership functions are derived. The output membership function is shown in Fig.16 below.

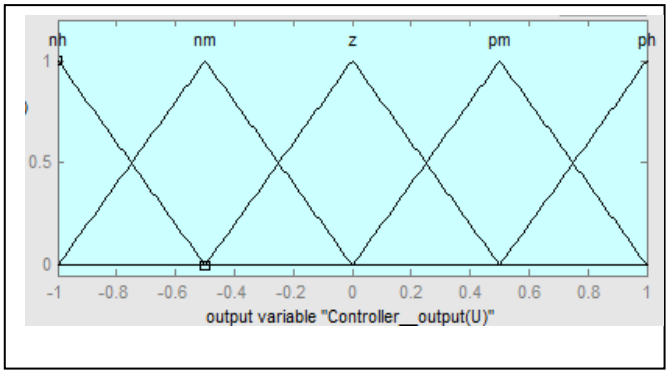

Fig.16. Membership Function of output function (U)

4.2.4 Defuzzification

In this paper frequently used by several authors the Center of Area defuzzification method (COA) is used to determine the final control input based on the inference result of each rule as described in Table-I.

4.3. Modeling of PWM controller

The output voltage of the VSI is controlled by the PWM technique by controlling the pulse width. The main aim of the PWM technique is to give maximum voltage and lowest harmonic distortion in the output waveform [24]. There are various types of PWM techniques that are available for the control of the VSI such as Sinusoidal PWM(SPWM), Space vector PWM, Selected harmonics elimination PWM(SHE) and Hysteresis Band Current Control PWM(HSCCPWM). In this paper a HBCC based PWM technique has been discussed for the control purpose of the Microgrid.

4.4. Hysteresis Band Current Controller PWM

Hysteresis band current controller is based on PWM techniques. This HBCC is generally used for many applications due to its simple mechanism and easy implementation. This controller is basically a current controlled method where the real current of the system tracks the reference current continuously inside the Hysteresis Band. It is an instantaneous feedback current controller. It has many advantages such as fast transient response during the parameter change conditions, ability to directly limit the device current, and insensitive to voltage ripple. The control circuit generates a reference wave form which is having certain amplitude and frequency. The actual current tracks that reference wave signal. When the actual current signal is more than the upper band limit then the switch is off, the voltage goes from +0.5 V_{dc} to -0.5V_{dc} . When the actual current crosses the lower band limit then the switch is on and at that time the voltage level goes from -0.5V_{dc} to +0.5V_{dc} [25]. The current error signals are fed as the input to the HBCC PWM to produce the pulse output. All the above cited mechanism are depicted in Fig.(17-18).

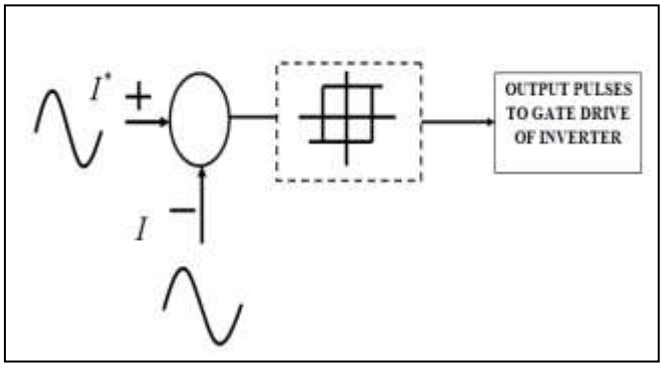

Fig.17. Control Block Diagram of Hysteresis Band Current Controller

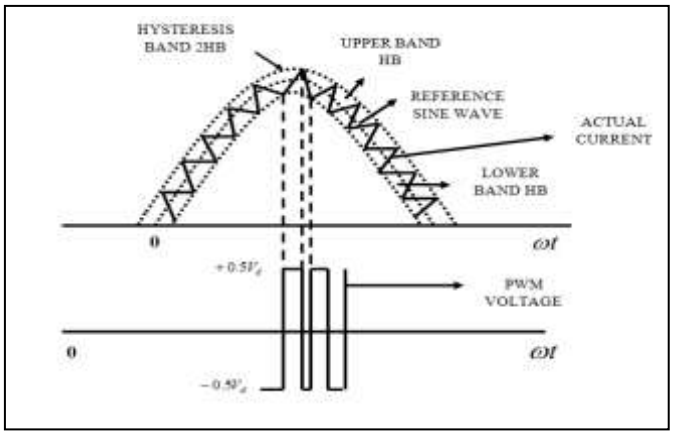

Fig.18. Principle of Hysteresis Band Current Controller

4.5 Structure of Adaptive PI controller

By implementing the equations related to various system components along with the fuel cells modeling as presented in Section 2 and 3, the dynamic model has been built in MATLAB/SIMULINK environment. The specifications and the value of the electrical model parameters of islanded Microgrid and SOFC used in the simulation studies are mentioned in Table-III and Table-IV respectively. The simulation time for all the tests in this study is taken as$T_s = 1\ X\ e^{-3}$. Four cases of dynamic analysis are performed on the system undertaken by implementing the proposed API control along with conventional PI and fuzzy control.

Case-I: Without Fault

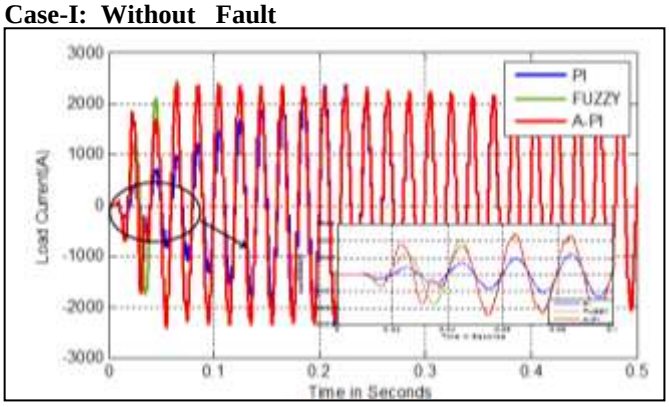

Fig.23. Load Current without Fault

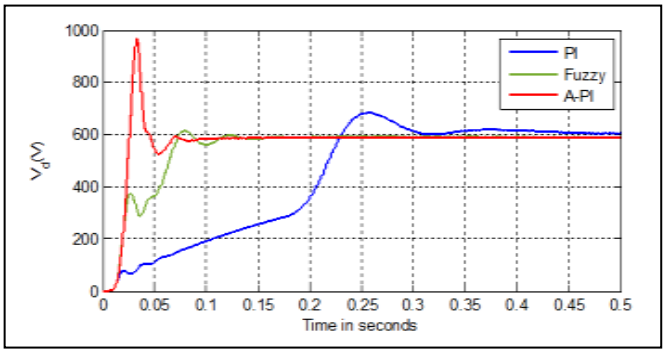

Fig.24. The d axis voltage without fault

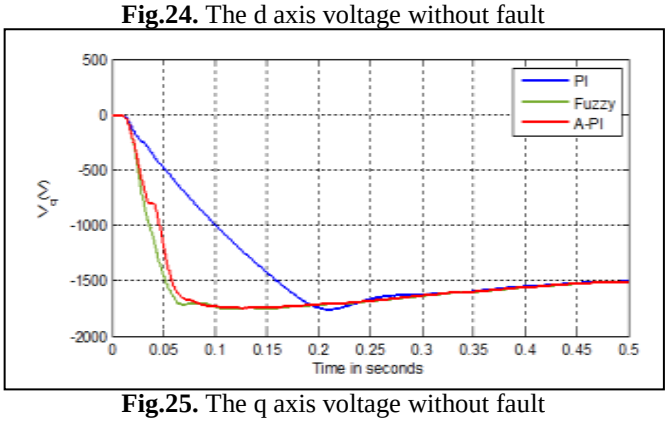

Fig.25. The q axis voltage without fault

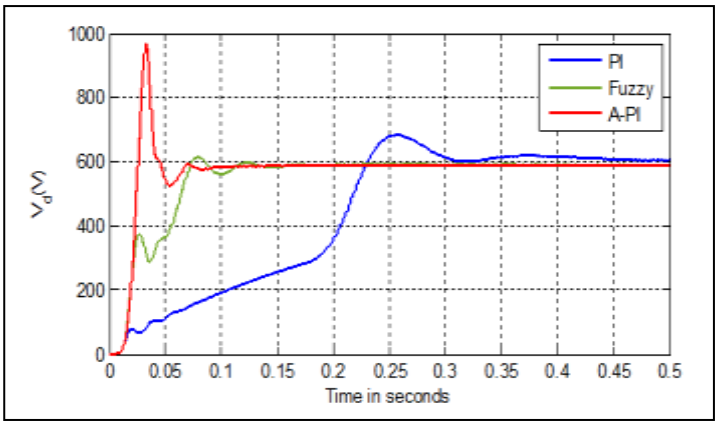

Fig.24. The d axis voltage without fault

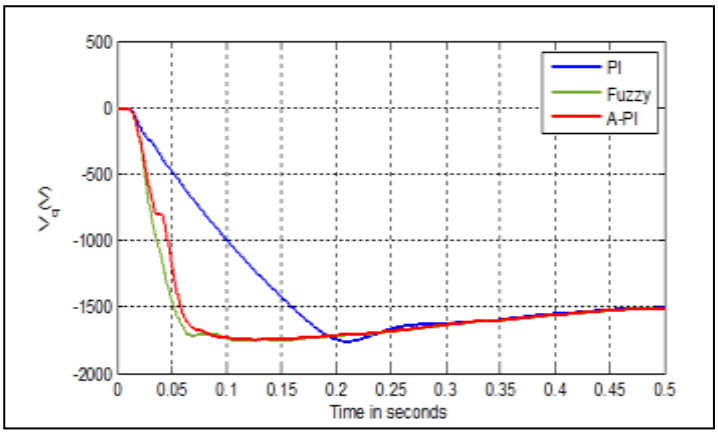

Fig.25. The q axis voltage without fault

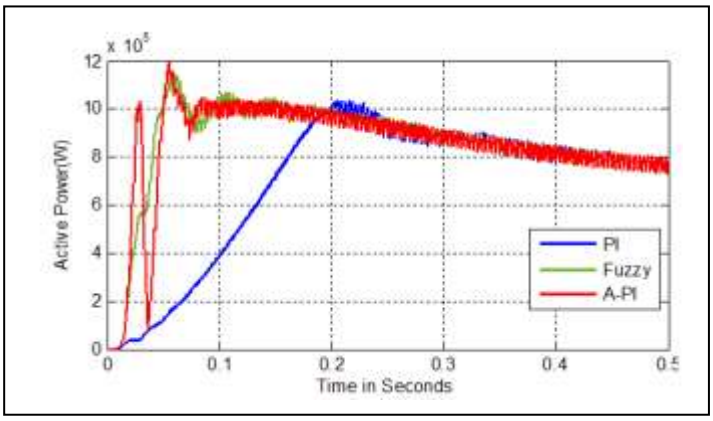

Fig.26. Active Power without Fault

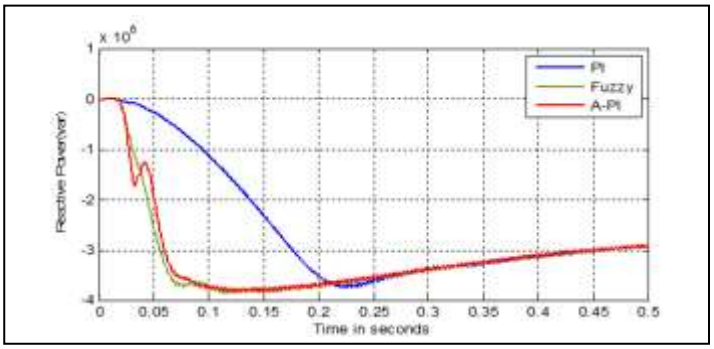

Fig.27. Reactive Power without Fault

Fig.23-27 shows the variation of load current, d-axis voltage, q-axis voltage, active power and reactive power respectively under no fault condition. In order to attain steady state value the load current takes 0.18 sec, 0.62 sec and 0.6 sec for the conventional PI, Fuzzy and API controller respectively as shown in Fig.23. The rise time of d-axis voltage is 0.074 sec, 0.225 sec and 0.026 sec for the PI, Fuzzy and API controller respectively as shown in Fig.24. The time taken to settle on optimum gains of the controllers in case of API, Fuzzy and PI controller are 0.033 sec, 0.08 sec and 0.255 sec respectively. Fig.25 depicts the q-axis voltage where the rise time of Fuzzy and proposed controller is 0.06 sec and 0.04 sec and slightly more in case of the PI controller takes 0.19 sec. The 0.215 sec peak time of q-axis voltage is very high for PI controller as compared to 0.07sec in case of the fuzzy and API controller. Similarly the settling time of PI controller is also very high (0.24 sec) on comparison to fuzzy and API controller (0.08 sec). Fig.26 shows the active power of the system, the rise time of PI controller is 0.23sec but for Fuzzy and API it is 0.055 sec and 0.052sec respectively. Comparing the peak time the PI controller gets its peak value at 0.24sec but in case of Fuzzy and API it is only 0.057sec and 0.055sec respectively. In Fig.27 the reactive power of the islanded system is taken into consideration, the PI controller takes 0.145sec more than the Fuzzy controller and API only takes 0.065 sec to reach the 90% value. Comparing the peak time the PI controller takes 0.225 sec but Fuzzy and proposed controller has much lower peak time as 0.09 and 0.075 respectively. The PI controller also has a large settling time of 0.27 sec. From all the figures it can clearly studied that the proposed controller has less rise time, less steady state error, better settling time, and quicker response.

Case-II: With Load Variation

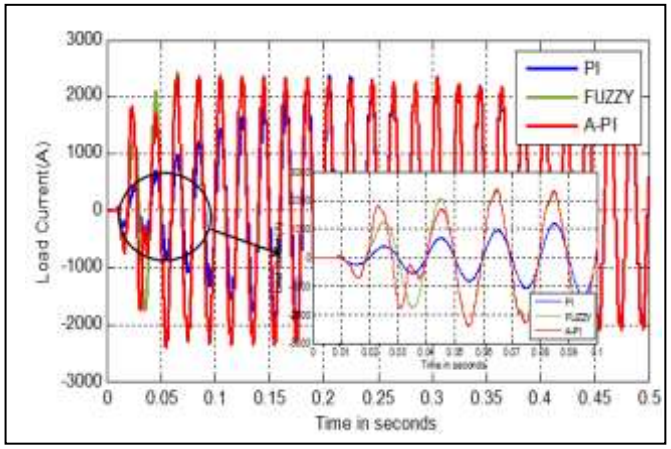

Fig.28. Load Current with load variation

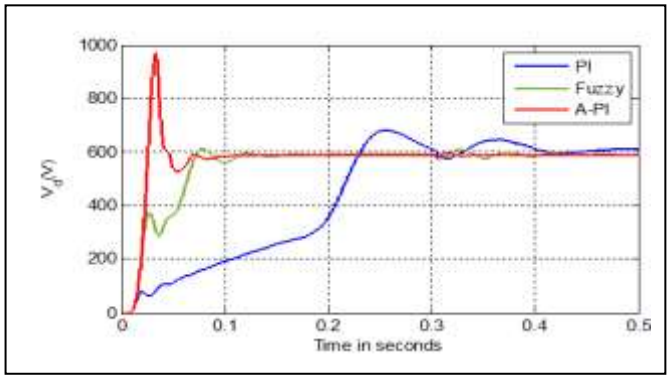

Fig.29. The d-axis Voltage with load variation

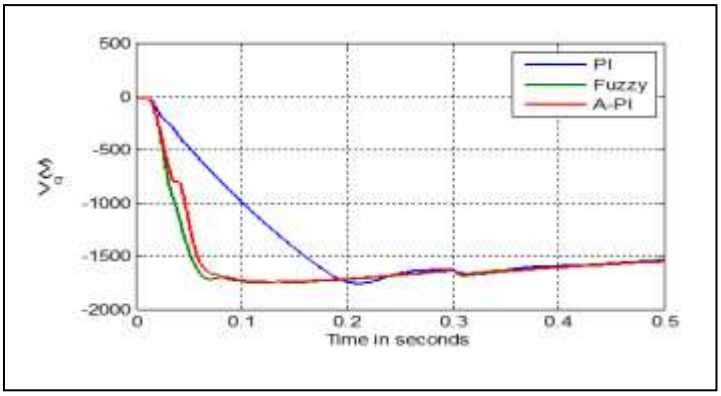

Fig.30. The q-axis Voltage with load variation

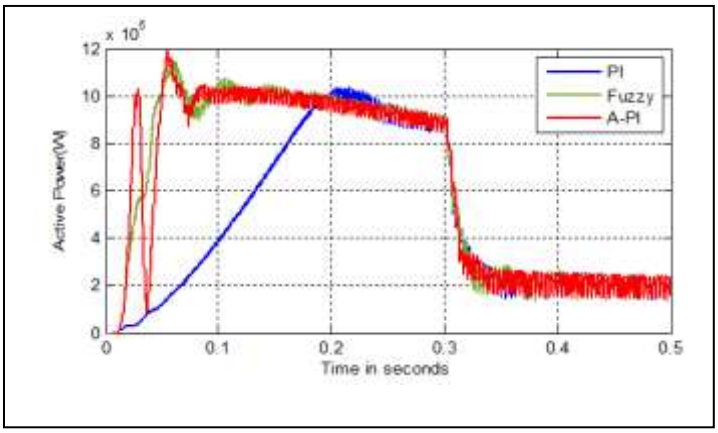

Fig.31. Active Power with Load variation

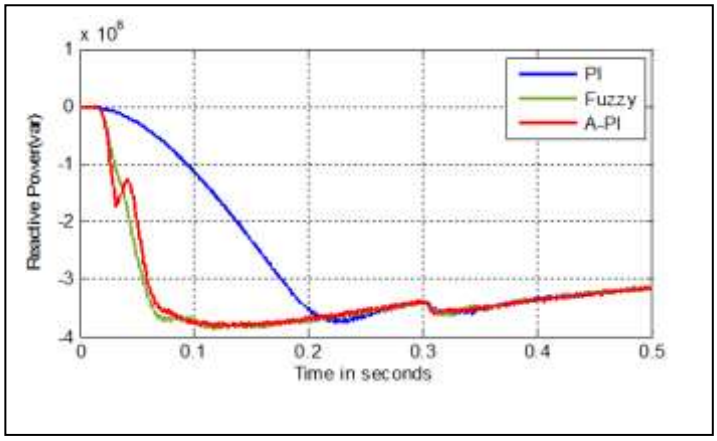

Fig.32. Reactive Power with Load Variation

Fig.28-32 shows the load current, d-axis voltage, q-axis voltage, active Power and reactive power respectively. Here a step change in load resistance is done which is varied from 5Ω to 20Ω. In case of load current to attain the steady state value the API responds better than PI and Fuzzy by 0.121 sec and 0.011 sec respectively as shown in Fig.28. Fig.29 represents the d-axis voltage where the API and Fuzzy controller has the rise time of 0.06 sec and 0.04 sec but the conventional PI controller takes almost double time. The above figures illustrates that the conventional PI controller and Fuzzy has high peak overshoot, high steady state error,

less rise time and settling time as compared to that of the proposed API controller.

Case-III: With Voltage Change

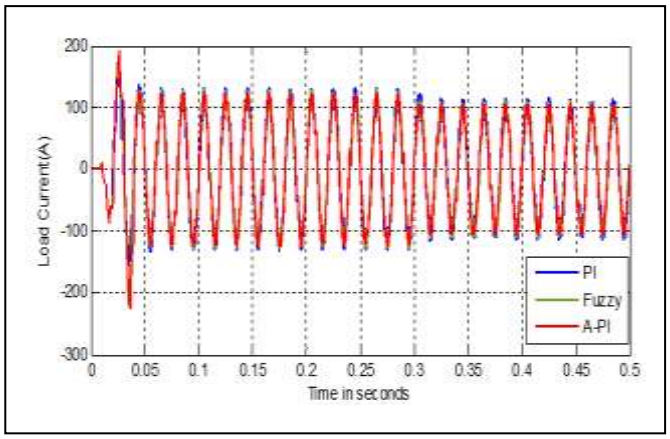

Fig.33. Load Current with voltage Change

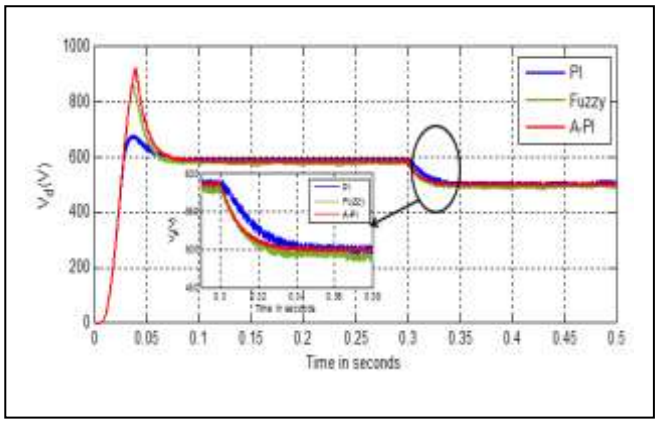

Fig.34. The d-axis Voltage with voltage change

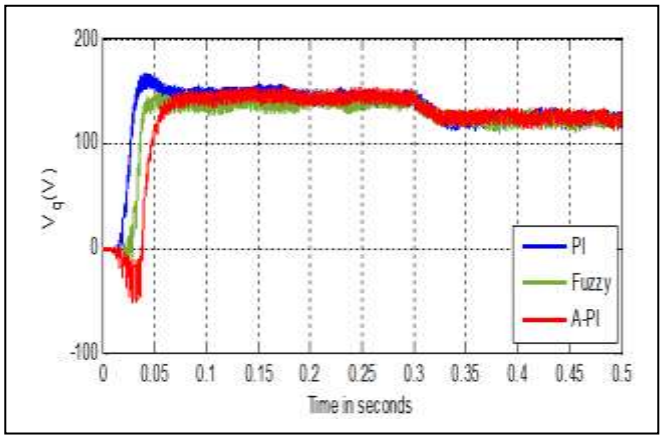

Fig.35. The q-axis Voltage with voltage change

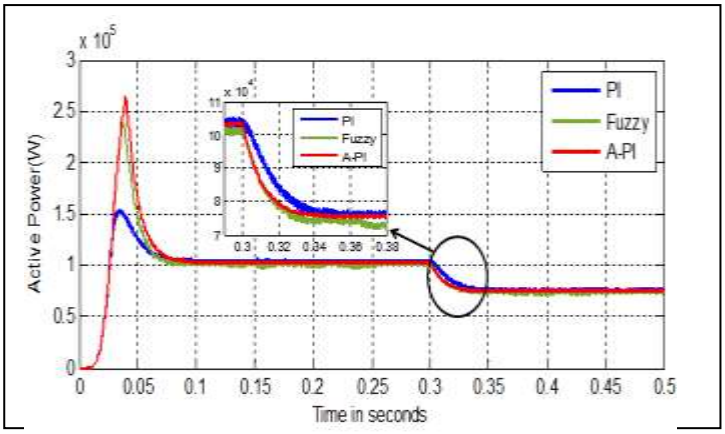

Fig.36. Active Power with voltage change

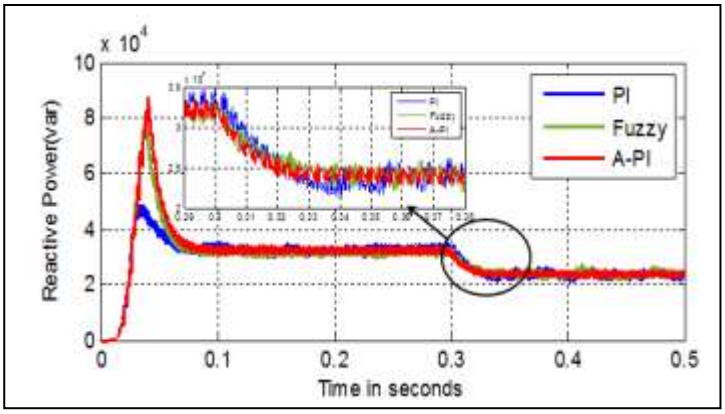

Fig. 37. Reactive Power with Voltage Change

Fig.33-37 shows the load current, d-axis voltage, q-axis voltage, active power and reactive power respectively during change in reference voltage. During the voltage change the proposed controller regains the steady state value in 0.015 sec where as fuzzy controller takes 0.025 sec and the conventional PI controller takes 2 times more than the proposed controller. Fig.33 depicts the q-axis voltage where the PI controller has an over shoot of 10% but it is only 7% and 2% in case of Fuzzy and API controller respectively. From all the above figures it can be clearly concluded that the proposed API controller has a much better settling time, less over shoot and no oscillations.

Case-IV: Non linear load switching

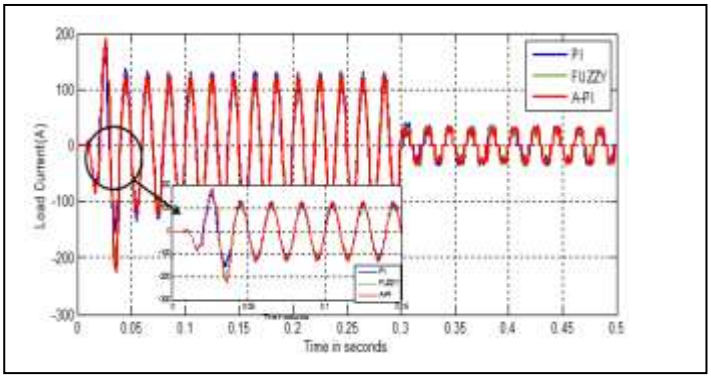

Fig.38. Load Current with nonlinear load switching

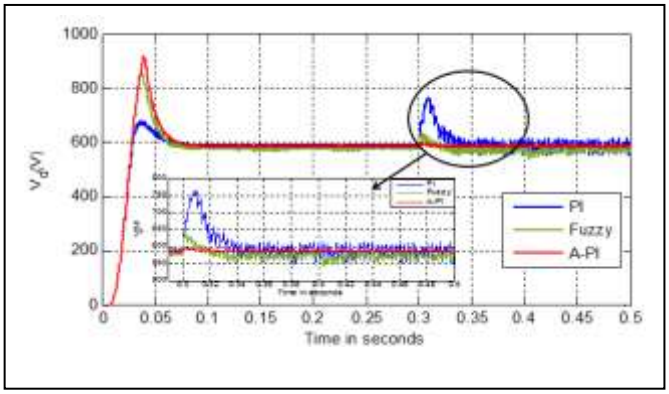

Fig.39. The d-axis Voltage with non linear load switching

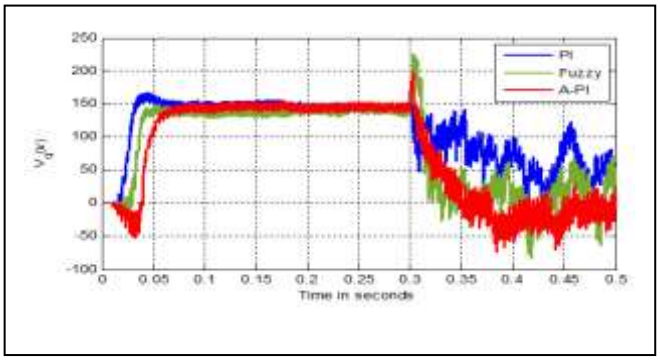

Fig.40. The q- axis voltage with non linear load switching

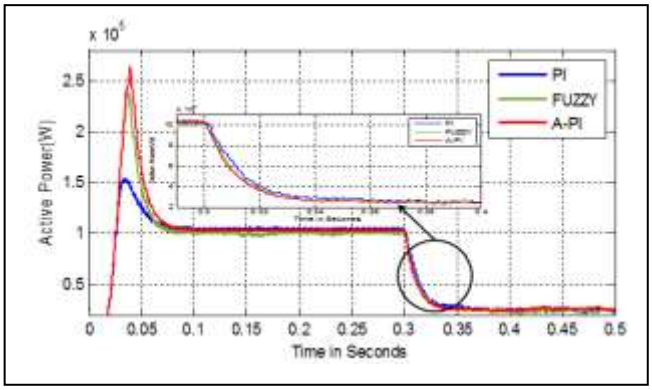

Fig.41. Active Power with non linear load switching

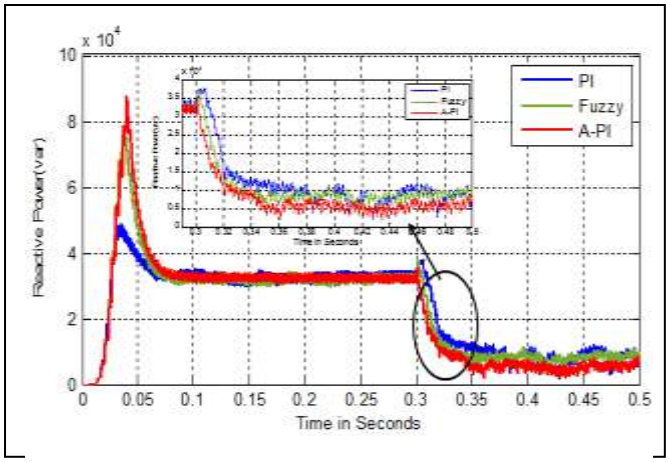

Fig.42. Reactive Power with non linear load switching

Fig.38-42 shows the load current, d-axis voltage, q-axis voltage, active power and reactive power respectively during non linear load switching. At 0.3 sec a non linear load (3-phase rectifier load) is switched on. Due to the nonlinear load the system becomes unstable but the proposed API controller acts very efficiently. For the d-axis voltage after the nonlinear load switching the API attains the steady state value within 0.005 sec but for the fuzzy and conventional PI controller it is 4 times and 7 times more than the API controller respectively. The PI controller has a very large over shoot of 31% but it is 6.89% in case of Fuzzy controller and for API controller it is almost negligible as shown in Fig.38. Fig.40. shows the active power of the system where after nonlinear load switching the PI controller has a settling time of 0.055 sec where as it is only 0.032 sec and 0.028 sec in case of Fuzzy and API controller respectively. The above results suggest that the API controller is more effective for controlling the islanded voltage even under load variability. Also the dynamic responses of the system with the proposed API controller have better transient behavior, damping, rise time, settling time and lower overshoot.

4. Conclusion

In this paper a distributed generation plant based on SOFC connected to the Microgrid environment in islanded mode of operation has been modeled and simulated using MATLAB/SIMULINK and to design the fuzzy controller MATLAB Fuzzy Logic Toolbox is used. An adaptive fuzzy PI controller is designed and tested in this system. In this control strategy the gains of the PI controller are found out by fuzzy logic by taking both error and change of error. In addition HBCC concept is implemented for the enhanced performance of PWM operation. The simulation results demonstrate the characteristics and responses of various system parameters including load current, active and reactive power, d-axis and q-axis voltage and gains of the controllers under linear and non-linear load variations. The comparative demonstrations of the proposed controller w.r.t conventional PI and fuzzy controller show a better closed loop performance and guarantees a robust stability and efficient performance irrespective of the load and voltage uncertainty.

Appendix

Table-3.. Parameters of the Islanded Microgrid system

PARAMETERS	VALUES
DC-link Voltage (V_{dc})	1500V
Fundamental Frequency(f)	50Hz
Filter Inductance(L_f)	1mH
Load Resistance(R)	5Ω
Load Inductance(L)	4mH
Power Factor	0.95 lagging
Active Power(P)	108KW
Reactive Power(Q)	32 Kvar
Kp,Ki	0.005,30

Table-4.SOFC Data

PARAMETERS	VALUES
SOFC Stack Output Voltage	807 V
SOFC Stack Output Current	70 A
SOFC Stack Output Power	60 KW
SOFC Stack Output Voltage After Boost	1500 V
SOFC Stack Output Current After Boost	66 A
SOFC Stack Output Power After Boost	100 KW
Number Of cells in series	675

References

[1] Lasseter, Robert H. "Microgrids." *Power Engineering Society Winter Meeting, 2002. IEEE*. Vol. 1. IEEE, 2002.

[2] Lasseter, Robert H. "Smart distribution: Coupled microgrids." *Proceedings of the IEEE* 99.6 (2011): 1074-1082.

[3] Piagi, Paolo, and Robert H. Lasseter. "Autonomous control of microgrids."*Power Engineering Society General Meeting, 2006. IEEE*. IEEE, 2006.

[4] Mudi, Rajani K., and Nikhil R. Pal. "A robust self-tuning scheme for PI-and PD-type fuzzy controllers." *Fuzzy Systems, IEEE Transactions on* 7.1 (1999): 2-16

[5] Blaabjerg, Frede, and Stig Munk-Nielsen. "Power losses in PWM-VSI inverter using NPT or PT IGBT devices." *Power Electronics, IEEE Transactions on*10.3 (1995): 358-367.

[6] Heldwein, M. L., T. Nussbaumer, and J. W. Kolar. "Differential mode EMC input filter design for three-phase AC-DC-AC sparse matrix PWM converters." *Power Electronics Specialists Conference, 2004. PESC 04. 2004 IEEE 35th Annual*. Vol. 1. IEEE, 2004.

[7] Elrayyah, Ali, Yilmaz Sozer, and Malik Elbuluk. "A robust and efficient PLL algorithm for single-phase grid-connected renewable energy sources."*Applied Power Electronics Conference and Exposition (APEC), 2013 Twenty-Eighth Annual IEEE*. IEEE, 2013.

[8] Reatti, Alberto, and Marian K. Kazimierczuk. "Small-signal model of PWM converters for discontinuous conduction mode and its application for boost converter." *IEEE Transactions on Circuits and Systems I: Fundamental Theory and Applications* 50.1 (2003): 65-73.

[9] Larminie, James, Andrew Dicks, and Maurice S. McDonald. *Fuel cell systems explained*. Vol. 2. New York: Wiley, 2003.

[10] Costamagna, Paola, Paolo Costa, and Vincenzo Antonucci. "Micro-modeling of solid oxide fuel cell electrodes." *Electrochimica Acta* 43.3 (1998): 375-394.

[11] Li, Xianguo, L. Fields, and G. Way. "Principles of fuel cells." *Platinum Metals Rev* 50.4 (2006): 200-1.

[12] Rocabert, Joan, et al. "Control of power converters in AC microgrids." *Power Electronics, IEEE Transactions on* 27.11 (2012): 4734-4749.

[13] Basak, Prasenjit, et al. "A literature review on integration of distributed energy resources in the perspective of control, protection and stability of microgrid."*Renewable and Sustainable Energy Reviews* 16.8 (2012): 5545-5556.

[14] Kanellos, F. D., Al I. Tsouchnikas, and N. D. Hatziargyriou. "Micro-grid simulation during grid-connected and islanded modes of operation."*International Conference on Power Systems Transients*. Vol. 6. 2005.

[15] Karimi, Houshang, Hassan Nikkhajoei, and Reza Iravani. "Control of an electronically-coupled distributed resource unit subsequent to an islanding event." *Power Delivery, IEEE Transactions on* 23.1 (2008): 493-501.

[16] Laaksonen, Hannu, Pekka Saari, and Risto Komulainen. "Voltage and frequency control of inverter based weak

LV network microgrid." *Future Power Systems, 2005 International Conference on*. IEEE, 2005.

[17] Lopes, J., C. L. Moreira, and A. G. Madureira. "Defining control strategies for microgrids islanded operation." *Power Systems, IEEE Transactions on* 21.2 (2006): 916-924.

[18] O'Dwyer, Aidan. *Handbook of PI and PID controller tuning rules*. Vol. 57. London: Imperial College Press, 2009

[19] Homaifar, Abdollah, and Ed McCormick. "Simultaneous design of membership functions and rule sets for fuzzy controllers using genetic algorithms." *Fuzzy Systems, IEEE Transactions on* 3.2 (1995): 129-139.

[20] Qiao, Wu Zhi, and Masaharu Mizumoto. "PID type fuzzy controller and parameters adaptive method." *Fuzzy sets and systems* 78.1 (1996): 23[68] Ying, Hao. *Fuzzy control and modeling: analytical foundations and applications*. Wiley-IEEE Press, 2000.

[21] Hasanien, Hany M., and Mahmoud Matar. "A fuzzy logic controller for autonomous operation of a voltage source converter-based distributed generation system." *Smart Grid, IEEE Transactions on* 6.1 (2015): 158-165.

[22] Qiao, Wu Zhi, and Masaharu Mizumoto. "PID type fuzzy controller and parameters adaptive method." *Fuzzy sets and systems* 78.1 (1996): 23[68] Ying, Hao. *Fuzzy control and modeling: analytical foundations and applications*. Wiley-IEEE Press, 2000.

[23] Mudi, Rajani K., and Nikhil R. Pal. "A self-tuning fuzzy PI controller." *Fuzzy sets and systems* 115.2 (2000): 327-338.

[24] Holmes, D. Grahame, and Thomas A. Lipo. *Pulse width modulation for power converters: principles and practice*. Vol. 18. John Wiley & Sons, 2003..

[25] Brod, David M., and Donald W. Novotny. "Current control of VSI-PWM inverters." *Industry Applications, IEEE Transactions on* 3 (1985): 562-570.

[26] Walter. Daugherity , Balaji Rathakrishnan, John Yen, "*Performance Evaluation Of A Self Tuning Fuzzy Controller",0-7803-0236-2/92, 1992 IEEE*